




Cite this: *RSC Adv.*, 2020, 10, 3566

Rapid synthesis of hierarchical SSZ-13 zeolite microspheres *via* a fluoride-assisted *in situ* growth route using aluminum isopropoxide as aluminum source†

Liancheng Bing,  Jiajia Liu, Kaifeng Yi, Fangni Li, Dezhi Han,  Fang Wang and Guangjian Wang*

Hierarchical SSZ-13 zeolite microspheres were quickly synthesized by adding a small quantity of hydrofluoric acid in the starting gel using aluminum isopropoxide as aluminum source. The as-synthesized hierarchical SSZ-13 crystals with high crystallinity, pore volume and external surface area were obtained within 12 h, whereas a much longer time (144 h) was necessary to synthesize a fully crystalline zeolite in a fluorine free system. The obtained hierarchical SSZ-13 catalysts showed excellent MTO performance together with considerably prolonged catalytic lifetime and improved selectivity of light olefins in comparison with the conventional microporous SSZ-13.

Received 29th October 2019
Accepted 12th January 2020

DOI: 10.1039/c9ra08895d

rsc.li/rsc-advances

Introduction

Zeolites with unique microporous structure and acidity have been widely used in the petrochemical industry as heterogeneous catalysts.^{1–3} As a successful non-petrochemical route to produce light olefins, the methanol-to-olefin (MTO) process over zeolite catalysts has received widespread attention and has undergone considerable development over the past few decades.⁴ To date, various zeolite catalysts have been used for the conversion of methanol, among which SSZ-13 zeolite with CHA framework topology exhibits high MTO catalytic performance, mostly contributed to its large surface area, useful pore structure in terms of shape selectivity, moderate acidity, and high thermal/hydrothermal stability.^{5–7} However, the mass transfer limitation and coke species formation in the cages result in a low catalytic efficiency and the rapid deactivation of SSZ-13.⁸

In order to prolong the catalytic lifetime and suppress the deactivation of SSZ-13 catalyst in the MTO reaction, various methods have been used to decrease the crystal size, which can significantly reduce the diffusion path length and enhance the accessibility of reactants to the external active sites.^{9,10} However, low crystallinity, low product yield, and difficulty in the separation of nanosized particles from reaction mixture are main

obstacles in industrial applications.¹¹ Recently, great efforts have been paid in the synthesis of hierarchical SSZ-13 zeolites, offering the combined advantages of both microporous crystals and mesoporous systems. This hierarchical structure can provide efficient mass transfer and improved accessibility of reactant molecules to the catalytically active sites on the premise of preserving shape selectivity, high thermal/hydrothermal stability and acid strength.^{12,13} Typical strategies for the preparation of hierarchical zeolite materials, such as alkaline treatment, does not enhance MTO catalytic performance when applied to SSZ-13, because of the decrease of surface area and acid sites.^{7,12} Hensen *et al.*^{13,14} synthesized mesoporous SSZ-13 crystals by a dually structure-directing synthetic route using *N,N,N*-trimethyl-1-adamantanammoniumhydroxide (TMAdOH) and diquatary ammonium type surfactant as templates. They further synthesized hierarchical SSZ-13 zeolites by adding surfactant C_{22–4–4}Br₂ and sodium fluoride to the synthesis gel.¹⁵ The obtained SSZ-13 zeolites featured not only native micropores characteristic of ordinary zeolites with CHA topological structure but also an additional micropore system with the average pore size of *ca.* 0.5 nm as well as mesopores. The hierarchical SSZ-13 catalysts exhibited remarkably prolonged catalyst lifetime in the MTO reaction compared to the conventional micropore catalyst at similar ethylene and propylene yields. However, the use of expensive reagents and complicated procedures as well as long reaction time (≥ 6 days at 160 °C) to form a hierarchical network not only increases the cost but also consumes much energy.^{14,16,17} Thus effectively shortening the crystallization time using simple and cost-effective synthetic procedure is of great practical significance.

State Key Laboratory Base for Eco-Chemical Engineering in College of Chemical Engineering, Qingdao University of Science and Technology, Qingdao 266042, China. E-mail: wgjnet@126.com

† Electronic supplementary information (ESI) available: More details of crystallization curves, XRD analyses, SEM, TEM, textural properties, pore size distribution, and the detailed MTO results over SSZ-13 catalysts. See DOI: 10.1039/c9ra08895d



Herein, we have developed a simple and fast synthetic method to prepare hierarchically porous SSZ-13 *via* adding a small quantity of hydrofluoric acid in the starting gel using aluminum isopropoxide as aluminum source. The addition of hydrofluoric acid into the initial synthesis gel obviously shorten the growth time of the crystal nucleus in the synthesis of hierarchical SSZ-13 zeolites. The as-synthesized SSZ-13 zeolites showed elliptical morphology comprising intracrystalline parallel meso-channels. The obtained hierarchical SSZ-13 catalysts showed outstanding MTO catalytic performance with a prolonged catalytic lifetime and improved selectivity of light olefins.

Experimental

Chemical and materials

Fumed silica was obtained from Sigma Aldrich. *N,N,N*-Trimethyl-1-adamantylammonium hydroxide (TMAdaOH, 25 wt%) was supplied by Hangzhou ICH Biofarm Co. Sodium hydroxide, aluminum isopropoxide (AIP), aluminum nitrate, sodium hydroxide, ammonium chloride, and hydrofluoric acid (HF, 40 wt%) were reagent grade from Sinopharm Chemical Reagent Co. All chemical reagents were analytical grade and were used without additional purification.

Hierarchical SSZ-13 synthesis

Hierarchical SSZ-13 zeolites were prepared using *in situ* growth route. The molar composition of the gel was Al_2O_3 : 40 SiO_2 : 4 TMAdaOH: 4 Na_2O : 1760 H_2O : 3.3 HF. First, NaOH was added into a 3-neck flask containing deionized water and stirred until dissolution. Then, TMAdaOH was added under vigorous stirring, which was then magnetic stirred for another 30 min to homogenize the organic and aqueous phases. After that, AIP as alumina source was added and continuously stirred at 28 °C for 1 h in order to obtain a clear resultant solution. Subsequently, an optimum amount of fumed silica was added slowly into the previously prepared solution, which was then magnetic stirred at room temperature for another 4 h. Finally, a certain amount of 40 wt% HF solution was added and then stirred for another 30 min. The resultant gel was sealed in a Teflon-lined steel autoclave and heated in a 160 °C oven at under static conditions for 6–48 h. After cooling down to room temperature, the obtained solid-like products were separated by centrifugation, washed with deionized water for several times, and dried overnight at 80 °C. After that, the powder samples were calcinated at 550 °C for 10 h to remove the organic template. All samples were exchanged with 2 mol L^{-1} NH_4Cl solution under stirring at 80 °C for three times to obtain NH_4 -type SSZ-13. After dryness, the solids were calcinated at 500 °C for 4 h. The obtained H-type SSZ-13 catalysts are denoted as SH-*x*, where *x* represents crystallization time.

Conventional SSZ-13 crystals synthesis

As reported in our previous work,¹⁸ conventional microporous SSZ-13 crystals were synthesized from the starting gel with a molar composition of Al_2O_3 : 40 SiO_2 : 4 TMAdaOH: 4 Na_2O :

1760 H_2O under conventional hydrothermal conditions at 160 °C for 48–144 h. Aluminum isopropoxide and aluminum nitrate were used as aluminum sources, respectively. The synthesis process for these zeolite crystals was similar to that of the system for synthesizing hierarchical SSZ-13 crystals without using HF. The synthesized SSZ-13 using aluminum nitrate as aluminum source are denoted as SM-*x*, where *x* represents the crystallization time; whereas SSZ-13 using aluminum isopropoxide as aluminum source is denoted as SAP.

Characterization

Powder X-ray diffraction (XRD) patterns were recorded on a Rigaku D/max 2500 diffractometer in the 2 theta angle range of 5 to 60° using Cu K α radiation. The crystal morphology and size of the obtained samples were identified on a JEOL JEM-2100 electron microscope. Transmission electron microscopy (TEM) images were obtained on a JEM-2100 instrument operating at 200 kV. Nitrogen adsorption/desorption experiments were carried out on a Micromeritics ASAP 2010M system at –196 °C. The samples were degassed at 250 °C for several hours before measurement. The specific surface area (S_{BET}) was determined based on the BET equation. The *t*-plot methods were used to determine the external surface area (S_{external}), micropore surface area (S_{micro}) and micropore volume (V_{micro}). The mesoporous volume (V_{meso}) was calculated by the BJH method to the adsorption isotherm. The element analysis was carried out by inductively coupled plasma atomic absorption spectroscopy (ICP-OES) using PerkinElmer Optima 2100 DV instrument. The acidity of the samples was measured by NH_3 -TPD using a Micromeritics Autochem II 2920 chemisorption analyser equipped with TCD as a detector under He flow. 50 mg of the calcinated sample was loaded into a U-tube. The packed column was purged at 350 °C under the stream of helium for activation. The sample was saturated with ammonia after the temperature decreased to 100 °C. Subsequently, the sample was flushed with a He flow for 30 min to remove the physically adsorbed NH_3 . Finally, the measurement of the desorbed NH_3 was performed from 100 to 700 °C (10 °C min^{-1}) in the presence of He flow. Solid state NMR experiments were carried out on a Tesla Bruker DMX500 NMR spectrometer. ^{27}Al MAS NMR spectra were recorded at 156.25 MHz with a 90° pulse length of 3.6 μs . Other parameters included a spinning frequency of 12.0 kHz and a recycle time of 5 s. ^{29}Si MAS NMR spectra were performed at 99 MHz with a spinning rate of 20 kHz and a pulse length of 2.2 μs with a 20 s repetition time.

Catalytic tests

Methanol conversion were performed at atmospheric pressure in a fixed-bed steel reactor with an inner diameter of 6 mm. 300 mg of calcinated catalyst (40–60 mesh) was loaded in the center of the quartz reactor in each run. Prior to the MTO reaction, the sample was activated at 500 °C for 1 h under an N_2 flow of 30 ml min^{-1} , and then decreased the temperature to 450 °C to carry out the reaction. Subsequently, methanol was introduced to the reactor by flowing N_2 (15 ml min^{-1}) through a saturator at 40 °C. The WHSV was kept at 3 h^{-1} . All products



from the reactors were analyzed on an online Agilent 6890 GC instrument equipped with a FID detector and a HP-PLOT Q capillary column.

Results and discussion

XRD patterns of the SSZ-13 crystals synthesized without using HF are shown in Fig. 1. In the conventional synthesis, the XRD pattern of the sample SM-48 crystallized for 48 h indicates that the solid product was essentially amorphous, although several very weak peaks were detected that can be associated with the CHA-type zeolite framework topology.^{13,19} An increased crystallization time from 48 to 144 h results in an gradually increased peak intensities, and crystallization completes after crystallization for 144 h, indicating the successful solid transformation of SSZ-13 zeolite crystals from the amorphous phase, confirmed by SEM (Fig. 2a and d). Fig. 3 shows XRD patterns of the hierarchical SSZ-13 synthesized with HF/Al₂O₃ of 3.3 at different crystallized time. The weak diffraction peaks associated with the CHA phase appear after 6 h of crystallization, which is interpreted by the initial crystal growth in the amorphous phase. The corresponding SEM image (Fig. 4d) indicates the formation of small amounts of zeolite particles. After the crystallization time reaches up to 12 h, the sample peak intensities increase greatly (Fig. 3), while the SEM image shows that the amorphous phase in the product disappears (Fig. 2b). After crystallization time over 12 h, no large change in the peak intensity is observed, indicating complete crystallization without any amorphous phase at 12 h, confirmed also by SEM (Fig. 2c, 4b and c). Fig. S1† shows the dependence of SSZ-13 crystallinity over the crystallization time, the addition of small amount of HF results in the reduction of the SSZ-13 synthesis time by 92% when compared with conventional counterpart synthesized without using HF. Moreover, the addition of HF and the crystallization time also affect the crystal size of the zeolitic products (Fig. 2 and 4). Some large cubic particles (8–9 μm) can be seen in the SEM images of SM-144 (Fig. 2a and d). When HF is added in the initial gel, the zeolitic product exhibits typical elliptical morphology with the average particle size of ca. 1–2 μm. The rough surfaces of the obtained particles might indicate that they are the aggregates of zeolite nanocrystals with abundant mesopores (Fig. 2e and f). The subsequent growth

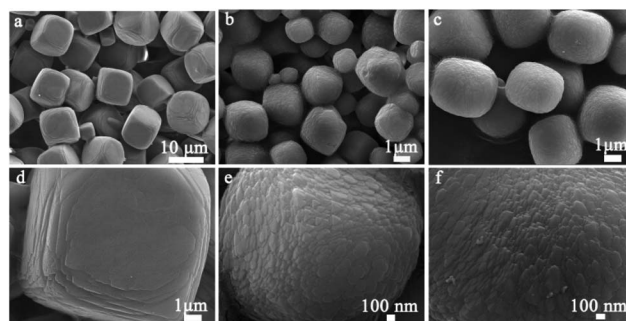


Fig. 2 SEM images of SSZ-13 samples: (a and d) SM-144; (b and e) SH-12; (c and f) SH-48. Scale bar: (a) 10 μm; (b–d) 1 μm; (e and f) 100 nm.

towards the elliptical morphology can be seen as the increase of crystallization time, and after crystallization for 48 h, the sample SH-48 shows larger particle size of ca. 3–4 μm, indicating that 12 h is enough to obtain fully crystallized SSZ-13 microspheres and probably the optimized value to completely transform to SSZ-13 zeolite with smaller crystal size. Fig. S2† shows the TEM image on the edge of a SH-12 microsphere. Bright areas can be seen in the image because of differences in thickness, indicating the existence of intracrystalline mesopores extending along the crystal in the hierarchical SH-12 zeolite microsphere.²⁰ In order to investigate the formation of aggregates of zeolite nanocrystals, SAP without HF was synthesized by using aluminum isopropoxide as aluminum source. As shown in Fig. S3,† the SAP zeolite shows a rough surface composed of 800 nm primary crystals, similar to that of the SH-12 and SH-48 samples. Therefore, the change of surface morphology of the SSZ-13 samples is attributed to the difference of aluminum source.

Fig. 5 displays the N₂ adsorption/desorption isotherms of the hierarchical SSZ-13 zeolites and the conventional counterpart. It can be seen that the sample SM-144 exhibits a standard type I adsorption isotherm typical of microporous zeolite materials without significant mesoporosity.^{21,22} In contrast to the sample SM-144, the addition of HF in the initial gel for samples SH-12 and SH-48 leads to an isotherm representing type IV behavior,²³ the large hysteresis loops in the 0.45 < *P*/*P*₀ < 0.95 partial pressure region is observed, indicating the presence of mesoporous structures formed by the aggregation of small crystallites. The

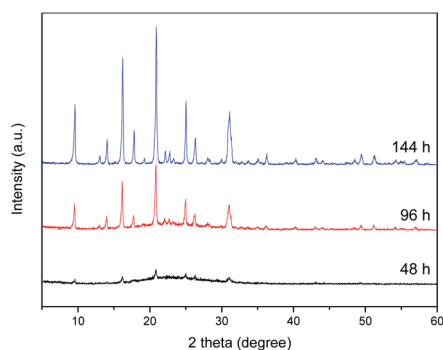


Fig. 1 XRD patterns of conventional SSZ-13 synthesized with different crystallization times.

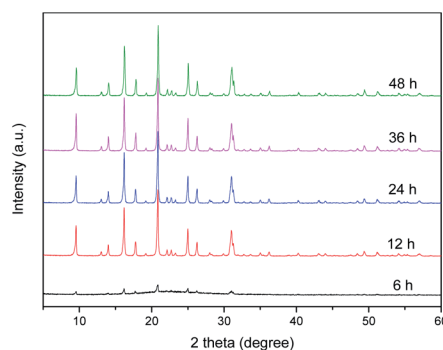


Fig. 3 XRD patterns of hierarchical SSZ-13 synthesized with different crystallization times.



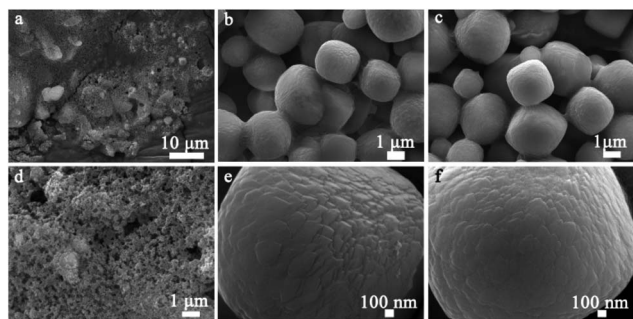


Fig. 4 SEM images of hierarchical SSZ-13 samples: (a and d) SH-6; (b and e) SH-24; (c and f) SH-36. Scale bar: (a) 10 μm ; (b–d) 1 μm ; (e and f) 100 nm.

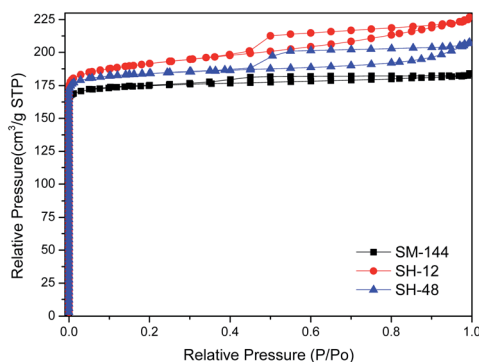


Fig. 5 N_2 adsorption/desorption isotherms of conventional microporous SSZ-13 and hierarchical SSZ-13 samples.

steep uptake at low partial pressure ($0 < P/P_0 < 0.01$) is still associate with the adsorption in the microstructure of the hierarchical SSZ-13 zeolites, which indicates that the formation of secondary pores does not decrease the micropore volume of the hierarchical SSZ-13 samples. Notably, compared with SH-48, SH-12 takes up N_2 in the low pressure range and the micropore adsorption capacity is also to be higher at high partial pressure. The textural properties of the crystals are summarized in Table S1.† The hierarchical SSZ-13 samples exhibit larger microporous volumes ($0.27\text{--}0.28\text{ cm}^3\text{ g}^{-1}$) than the conventional counterpart ($0.24\text{ cm}^3\text{ g}^{-1}$), which mainly resulted from the fact that a small amount of amorphous phase and/or defect zones in the conventional SSZ-13 is easy to be attacked.²⁴ This is in good agreement with the increase of crystallinity based on the analysis of XRD spectra as shown in Fig. S4.† The specific surface areas and mesoporous volumes of the hierarchical SSZ-13 samples ($559\text{--}591\text{ m}^2\text{ g}^{-1}$) are also increased, because of the increase of external surface area. The pore-size distribution also demonstrates the existence of mesopores centered at around 4 nm in samples SH-12 and SH-48 (Fig. S5†). The large mesoporous volume of hierarchical SSZ-13 samples would be beneficial for decreasing the diffusion limitation of reactants and products, with the corresponding effect on the MTO performance.^{25,26}

The Si/Al ratios of the hierarchical SSZ-13 samples measured by ICP (Table S1†) are similar to that of the conventional one synthesized without HF. The ^{27}Al MAS NMR spectra in Fig. 6a show that both SM-144 and SH-12 samples exhibit two peaks centered at chemical shifts of *ca.* 54 ppm and -2 ppm. The signals at *ca.* 54 ppm are assigned to tetrahedrally coordinated framework aluminum atoms.^{15,27} The relatively weak signals at *ca.* -2 ppm indicate the existence of a limited number of octahedrally coordinated extra framework aluminum species.^{28,29} Their levels in the SM-144 and SH-12 zeolite are however similar. Therefore, the introduction of HF does not change the extra framework aluminum species appreciably. The coordination environment of the Si atoms in SM-144 and SH-12 frameworks was characterized by ^{29}Si MAS NMR spectrum (Fig. 6b). Peaks at -113 , -107 , and -103 ppm are ascribed to Si(0Al), Si(1Al), and Si(2Al), respectively.³⁰ The distribution of Si(*n*Al) does not obvious change with the addition of HF, indicating that the sample SH-12 possesses almost similar coordination states of Si atoms compared to the conventional SSZ-13.

NH_3 -TPD curves of the hierarchical SSZ-13 zeolites and the conventional one are shown in Fig. 7. The conventional SSZ-13 exhibits two ammonia desorption peaks at *ca.* 140 and 490 $^\circ\text{C}$, corresponding to the weak and strong acid sites, respectively.^{31,32} Ammonia molecules desorbs before 300 $^\circ\text{C}$ from the weak acid sites. Thus, methanol as a less basic molecule cannot be able to be converted into light olefins at 450 $^\circ\text{C}$ on these sites. This means that weak acid sites have no evident effect on the MTO catalytic performance of SSZ-13 catalysts.³³ The high temperature desorption peaks corresponding to the interaction of NH_3

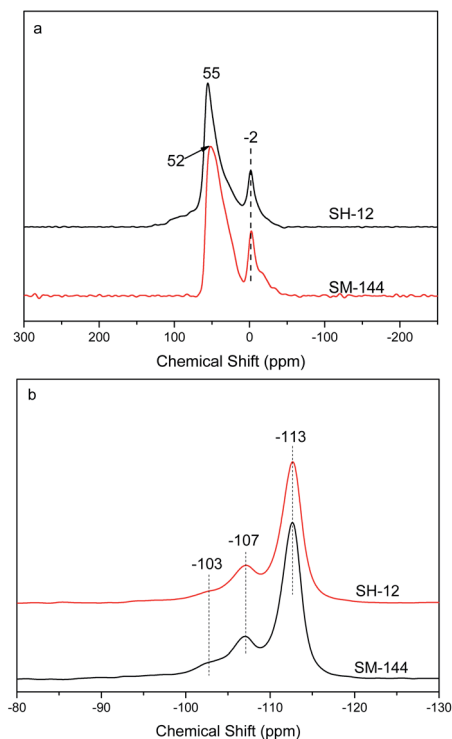


Fig. 6 (a) ^{27}Al MAS NMR and (b) ^{29}Si MAS NMR spectra of SSZ-13 samples.



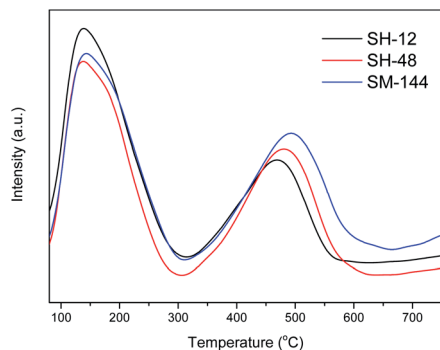


Fig. 7 NH_3 -TPD of conventional microporous SSZ-13 (SM-144) and hierarchical porous SSZ-13 (SH-12 and SH-48) catalysts.

molecules with strong acid sites are ascribed to the Brønsted acid sites that is connected with the MTO catalytic performance.³⁴ The NH_3 -TPD profiles of the hierarchical SSZ-13 samples are similar to that of the conventional microporous SSZ-13, but the position and intensity of the high temperature peak are slightly lower, indicating lower strong acidity for the hierarchical SSZ-13 zeolites compared to the conventional counterpart.

Catalytic reaction tests were carried out in a fixed-bed steel reactor at 450 °C with a WHSV of 3 h^{-1} over the conventional and hierarchical SSZ-13 catalysts. The catalytic conversions of methanol and selectivities of the products as a function of time-on-stream (TOS) are shown in Fig. 8 and S6–S8,[†] and the detailed catalytic results are summarized in Table S2.[†] Obviously, the initial methanol conversion for all catalysts is complete, and ethylene and propylene as the combined yield is

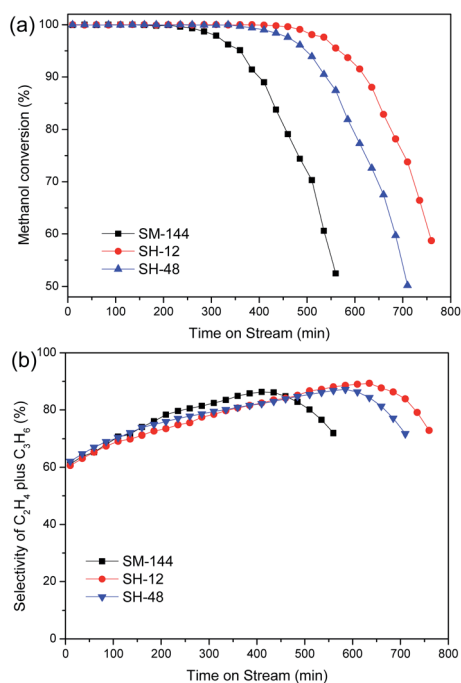


Fig. 8 Methanol conversion (a) and selectivity to ethylene plus propylene (b) with time-on-stream over SSZ-13 samples.

the main reaction products. Methanol conversion of the conventional microporous SSZ-13 synthesized without adding HF eventually decreases with the increase of TOS. The hierarchical SSZ-13 catalysts exhibit a remarkably longer lifetime than conventional counterpart with only microporous structure. The most stable catalyst is SH-12, which displays a lifetime of 485 min before the methanol conversion decreased to less than 99%. Notably, the catalytic activity of SH-48, hierarchical SSZ-13 synthesized with longer crystallization time, is better than that of SM-144 yet worse than that of SH-12. This proves that the use of the fluoride in the synthesis of SSZ-13 zeolite catalyst with shortened crystallization time is consistent with respect to MTO catalytic performance.

The high selectivity of light olefins is another important benefit of the use of MTO catalyst. The introduction of secondary porosity has been proven to improve the catalytic selectivity because of the greatly enhanced diffusion efficiency.^{15,26,35} As shown in Fig. S6–S8,[†] the selectivity data with >95% methanol conversion shows that ethylene plus propylene selectivity of hierarchical SH-12 (85.1%) is improved around 6% compared to the conventional microporous SM-144 (80.5%), and slightly higher than the hierarchical SH-48 (82.2%). The generated mesopore in the hierarchical SSZ-13 catalysts not only enhances the mass transfer of the reagents and products but also exposes more active sites for MTO reaction as well as reduce the coke deposition.^{13,36} In addition, the decrease of strength and concentration in strong acid sites of hierarchically structured SH-12 can also reduce the coke deposition. Furthermore, the decreased crystal size of the hierarchical SSZ-13 catalysts is another important reason for prolonging the lifetime. The smaller crystal size of sample SH-12 can shorten the diffusion pathway of reactants and products and suppresses the coke formation rate during the methanol conversion, and thus prolong the catalyst lifetime and enhance the light olefin selectivity.^{9,37} Above results demonstrate that the improved catalytic lifetime and light olefins selectivity of the hierarchical SSZ-13 catalysts can be attributed to the high crystallinity, the enhanced diffusion efficiency, the increased microporous volume and the appropriate acidity in strong acid sites of the hierarchically structured zeolite materials.

Conclusions

In summary, a simple, rapid and low-cost approach has been developed to synthesize hierarchical SSZ-13 by one-step hydrothermal synthesis method using aluminum isopropoxide as aluminum source with the assistance of HF. The as-synthesized hierarchical SSZ-13 crystals were highly crystalline, and the crystal growth process was completed within 12 h, whereas 144 h was necessary to synthesize a fully crystalline zeolite in fluorine free system. The hierarchical SSZ-13 catalysts showed higher micropore volume than the conventional microporous SSZ-13 synthesized without HF, and the assistance of HF could lead to the increase of specific surface areas and mesoporous volumes because of the increase of external surface area caused by the formation of mesopores. Taking advantage of the large micropore volume and accessible active sites, enhanced mass



transfer and reduced coke formation rate, and appropriate strong acidic strength and concentration, the hierarchical SSZ-13 catalysts exhibited enhanced light olefins selectivity as well as significantly prolonged catalyst lifetime as compared to the conventional micropore SSZ-13.

Conflicts of interest

There are no conflicts to declare.

Acknowledgements

The authors gratefully acknowledge financial support of this work by the Foundation of State Key Laboratory of High-efficiency Utilization of Coal and Green Chemical Engineering (2017-K17 and 2017-K23), the Shandong Provincial Natural Science Foundation, China (ZR2018027, ZR2019BB052), and the opening Project of Shandong Eco-chemical Engineering Collaborative Innovation Center (XTCXQN15).

Notes and references

- 1 B. Z. Zhan, M. A. White, T. K. Sham, J. A. Pincock, R. J. Doucet, K. V. R. Rao, K. N. Robertson and T. S. Cameron, *J. Am. Chem. Soc.*, 2003, **125**, 2195–2199.
- 2 M. Choi, K. Na, J. Kim, Y. Sakamoto, O. Terasaki and R. Ryoo, *Nature*, 2009, **461**, 246–249.
- 3 J. Kim, M. Choi and R. Ryoo, *J. Catal.*, 2010, **269**, 219–228.
- 4 P. Tian, Y. Wei, M. Ye and Z. Liu, *ACS Catal.*, 2015, **5**, 1922–1938.
- 5 F. Bleken, M. Bjorgen, L. Palumbo, S. Bordiga, S. Svelle, K. P. Lillerud and U. Olsbye, *Top. Catal.*, 2009, **52**, 218–228.
- 6 M. A. Deimund, L. Harrison, J. D. Lunn, Y. Liu, A. Malek, R. Shayib and M. E. Davis, *ACS Catal.*, 2016, **6**, 542–550.
- 7 X. Zhu, N. Kosinov, A. V. Kubarev, A. Bolshakov, B. Mezari, I. Valastyan, J. P. Hofmann, M. B. J. Roefsaers, E. Sarkadi-Pribóczy and E. J. M. Hensen, *ChemCatChem*, 2017, **9**, 3470–3477.
- 8 X. Zhu, N. Kosinov, J. P. Hofmann, B. Mezari, Q. Qian, R. Rohling, B. M. Weckhuysen, J. Ruiz-Martínez and E. J. M. Hensen, *Chem. Commun.*, 2016, **52**, 3227–3230.
- 9 Z. Li, M. T. Navarro, J. Martínez-Triguero, J. Yu and A. Corma, *Catal. Sci. Technol.*, 2016, **6**, 5856–5863.
- 10 C. Peng, Z. Liu, A. Horimoto, C. Anand, H. Yamada, K. Ohara, S. Sukenaga, M. Ando, H. Shibata, T. Takewaki, R. R. Mukti, T. Okubo and T. Wakihar, *Microporous Mesoporous Mater.*, 2018, **255**, 192–199.
- 11 Y. Shi, X. Li, J. Hu, J. Lu, Y. Ma, Y. Zhang and Y. Tang, *J. Mater. Chem.*, 2011, **21**, 16223–16230.
- 12 L. Sommer, D. Mores, S. Svelle, M. Stöcker, B. M. Weckhuysen and U. Olsbye, *Microporous Mesoporous Mater.*, 2010, **132**, 384–394.
- 13 L. Wu, V. Degirmenci, P. C. M. M. Magusin, N. J. H. G. M. Lousberg and E. J. M. Hensen, *J. Catal.*, 2013, **298**, 27–40.
- 14 L. Wu, V. Degirmenci, P. C. M. M. Magusin, B. M. Szyja and E. J. M. Hensen, *Chem. Commun.*, 2012, **48**, 9492–9494.
- 15 X. Zhu, J. P. Hofmann, B. Mezari, N. Kosinov, L. Wu, Q. Qian, B. M. Weckhuysen, S. Asahina, J. Ruiz-Martínez and E. J. M. Hensen, *ACS Catal.*, 2016, **6**, 2163–2177.
- 16 L. Wu and E. J. M. Hensen, *Catal. Today*, 2014, **235**, 160–168.
- 17 M. Kumar, H. Luo, Y. Román-Leshkov and J. D. Rimer, *J. Am. Chem. Soc.*, 2015, **137**, 13007–13017.
- 18 L. Bing, G. Wang, K. Yi, F. Li, J. Liu and F. Wang, *Catal. Lett.*, 2018, **148**, 2728–2733.
- 19 Z. Liu, T. Wakihara, K. Oshima, D. Nishioka, Y. Hotta, S. P. Elangovan, Y. Yanaba, T. Yoshikawa, W. Chaikittisilp, T. Matsuo, T. Takewaki and T. Okubo, *Angew. Chem., Int. Ed.*, 2015, **54**, 5683–5687.
- 20 C. Li, Y. Wang, B. Shi, J. Ren, X. Liu, Y. Wang, Y. Guo, Y. Guo and G. Lu, *Microporous Mesoporous Mater.*, 2009, **117**, 104–110.
- 21 D. Xi, A. Sun, J. Xu, M. Cho, H. S. Cho, S. Asahina, Y. Li, F. Deng, O. Terasaki and J. Yu, *J. Mater. Chem. A*, 2014, **2**, 17994–18004.
- 22 Y. Liu, L. Xu, Y. Lv and X. Liu, *J. Colloid Interface Sci.*, 2016, **479**, 55–63.
- 23 U. J. Etim, B. Xu, Z. Zhang, Z. Zhong, P. Bai, K. Qiao and Z. Yan, *Fuel*, 2016, **178**, 243–252.
- 24 S. Du, X. Chen, Q. Sun, N. Wang, M. Jia, V. Valtchev and J. Yu, *Chem. Commun.*, 2016, **52**, 3580–3583.
- 25 X. Zhu, R. Rohling, G. Filonenko, B. Mezari, J. P. Hofmann, S. Asahina and E. J. M. Hensen, *Chem. Commun.*, 2014, **50**, 14658–14661.
- 26 Q. Sun, N. Wang, G. Guo, X. Chen and J. Yu, *J. Mater. Chem. A*, 2015, **3**, 19783–19789.
- 27 F. Meng, X. Wang, S. Wang and Y. Wang, *Catal. Today*, 2017, **298**, 226–233.
- 28 T. Sonoda, T. Maruo, Y. Yamasaki, N. Tsunoji, Y. Takamitsu, M. Sadakane and T. Sano, *J. Mater. Chem. A*, 2015, **3**, 857–865.
- 29 A. K. Jamil, O. Muraza, M. H. Ahmed, A. Zainalabdeen, K. Muramoto, Y. Nakasaka, Z. H. Yamani, T. Yoshikawa and T. Masuda, *Microporous Mesoporous Mater.*, 2018, **260**, 30–39.
- 30 T. Yu, D. Fan, T. Hao, J. Wang, M. Shen and W. Li, *Chem. Eng. J.*, 2014, **243**, 159–168.
- 31 S. Xu, A. Zheng, Y. Wei, J. Chen, J. Li, Y. Chu, M. Zhang, Q. Wang, Y. Zhou, J. Wang, F. Deng and Z. Liu, *Angew. Chem., Int. Ed.*, 2013, **52**, 11564–11568.
- 32 W. Chooon and S. Jitkarnka, *J. Cleaner Prod.*, 2016, **135**, 368–378.
- 33 A. Izadbakhsh, F. Farhadi, F. Khorasheh, S. Sahebdehfar, M. Asadi and Z. F. Yan, *Appl. Catal., A*, 2009, **364**, 48–56.
- 34 Q. Qian, J. Ruiz-Martínez, M. Mokhtar, A. M. Asiri, S. A. Al-Thabaiti, S. N. Basahel and B. M. Weckhuysen, *Catal. Today*, 2014, **226**, 14–24.
- 35 H. Yang, Z. Liu, H. Gao and Z. Xie, *J. Mater. Chem.*, 2010, **20**, 3227–3231.
- 36 Q. Sun, N. Wang, R. Bai, X. Chen and J. Yu, *J. Mater. Chem. A*, 2016, **4**, 14978–14982.
- 37 S. Masoumi, J. Towfighi, A. Mohamadizadeh, Z. Kooshki and K. Rahimi, *Appl. Catal., A*, 2015, **493**, 103–111.